Postprint of: Kowalczuk Z., Tatara M.: Sphere Drive and Control System for Haptic Interaction With Physical, Virtual, and Augmented Reality IEEE TRANSACTIONS ON CONTROL SYSTEMS TECHNOLOGY Vol. 27, iss. 2 (2019), pp. 588-602
DOI: 10.1109/TCST.2017.2780057

Sphere Drive and Control System for Haptic Interaction with Physical, Virtual and Augmented Reality

Zdzisław Kowalczuk, *Senior Member, IEEE,* and Marek Tatara

***Abstract*—A system for haptic interaction with physical, virtual and augmented realities, founded on drive and measurement elements (DMEs), is considered. The system consists of 8 DME rolls equipped with linear actuators, able to measure their angular velocity, to drive the sphere and to adjust downforce (pressing the roll against the sphere). Two modeling issues are addressed. Special effort is put in to compensate for various technical issues. Analytic derivation of the relation between the angular velocities of the rolls and the sphere is presented. On this basis, the importance of control over the downforce applied to an individual roll is indicated with the aim of minimizing the wear of the roll. The selection of the proper downforce for each specific position (angle) of a DME roll can extend its life cycle by reducing its grinding on the sphere. The issue of modeling the relation between the angular velocity of a given DME and the sphere is addressed. In a simplified case, such a relation can be obtained analytically. However, for a nonuniform distribution of reaction forces on the contact area, a numerical approach is necessary. Two numerical methods for estimation of the angular velocity of the DME roll are presented and discussed. Moreover, an algorithm for estimation of the sphere's rotational motion parameters is described and implemented, proving the usefulness of the presented method.**

***Index Terms*—Haptic Interfaces, Tactile Sensing, Virtual Reality and Interfaces, Mechanism Design, Control and Measurement Equipment, Cyber-physical System, Remote Operation, Mobile Robotics, Smart Components, Scheduling Variable, Adaptive Systems.**

I. Introduction

INSTALLATION of a 5 foot radius sphere (Fig. 1) located in IVL - the Immersive 3D Visualization Lab [1], [2], [3], [4], [5] at the Gdańsk University of Technology has been an inspiration for the proposed industrial research and development having the aim of creating a spherical walk simulator with an intelligent drive for haptic control of a remote robotic land rover. The idea is to walk in augmented reality, using remote control of the mobile robot, which, equipped with a stereovision set of cameras, moves in a physical space. Touch interface means coupling with the ability to measure or influence the user's senses, for example by touching or moving [6]. There are systems that use haptic interface to virtual reality [7], [8], [9], or enable remote operation of a robot [10], [11], [12], but none of them combines the functionality of both. The entire target system falls under the definition of cyber-physical system [13], and the part presented in this paper concerns the design and simulation of measurement and control systems. The applied control loop is based on haptic feedback generated by a walker inside the sphere. The proposed system is to provide twofold haptic interaction: (1) by allowing the walker to feel the impression of traversing on the terrain through his/her feet while moving in the sphere, and (2) by reflecting different terrain shapes by making it more difficult or easier to move. In the system it is thus possible to actively simulate the various stresses that occur between the walker and the terrain on which he/she moves. The standalone system, without intelligent drives, provides measurements of the walker's movement, required for tracking his/her position in virtual reality, via an optical device similar to the one used in computer mouses. However, the precision of these measurements is unsatisfactory. The existing standalone system provides measurements with long time delay between innovative samples, and the obtained estimates have high variance, which causes jumps in the estimated position of the user in the virtual reality. Moreover, the system does not allow one to influence externally the sphere's rotational motion (sphere is affected solely by the walker). There are other systems allowing to move within virtual reality: they can be sphere-shaped [14], or in the form of a treadmill [15], [16], [17], but none of them affects its user in the natural way. In the sphere-based systems, due to their inertia, the impression of walking can differ from the one experienced in reality. The problem of the natural walking inside such spheres is pointed out in [18], [19], where the proposed solutions improve the walker's interaction with the system or introduce additional measurement of movement direction, for instance from walker's torso. In view of the aforementioned facts, a need arises to design a driving and measurement system for estimation of the velocity and angle of the walker's movement (and tracking of the user's trajectory as a result) and for active driving of the sphere, making the experience of the simulated walk closer to the real one.

Z. Kowalczuk and M. Tatara are with the Department of Robotics and Decision Systems, Faculty of Electronics, Telecommunications and Informatics, Gdańsk University of Technology, Poland (e-mail: kova@pg.edu.pl; martatar@pg.edu.pl).

Manuscript received , ; revised , .

II. Description of the Proposed Drive System

The system consists of 8 drive and measurement elements (DMEs) - founded on enforcing rolls with linear actuators attached, distributed horizontally around the sphere every 45° (Fig. 2). The fixed-position rolls (interacting with the sphere) can work in a passive mode (PM), allowing one to measure their rotation speed, and in an active mode (AM)

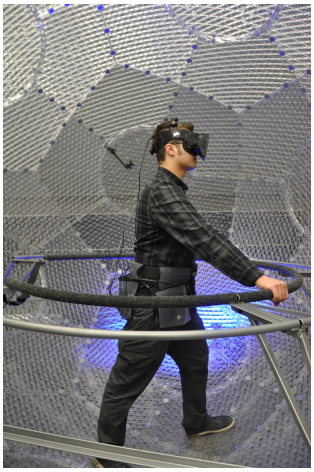

Fig. 1: View of a walker inside the sphere in the IVL laboratory, equipped with a virtual reality set.

allowing them to drive the sphere. Accordingly, two styles of the walker's motion can be distinguished: active walk (AW) with the rolls in PM or AM, when the system emulates different conditions of walk (making it harder or easier, or an impression of walking up or down the slope) or passive walk (PW) with rolls in AM, forcing the movement of the walker in a particular direction at a specified speed (as a retrace of a previously programmed trajectory).

Each DME has a linear motor with force feedback to smoothly control the utilitarian downforce on the rolls in both modes. Adequately to its location, DME should be able to measure a corresponding component of the linear velocity of the sphere (more precisely – to provide information about the spherical motion), inside of which a person is walking. This effect is obtained by measuring the angular velocity of the roll, which can also be driven by its DME in AM. Proper elasticity of the roll's material is most essential. The roll's downforce ought to be adjustable between the maximum allowed by the material elasticity, efficiency of friction, and certain geometric assumptions (Fig. 3), and the minimum reducing the contact area of the roll and the sphere (CARS) to a minimum point (complete detachment of the roll from the sphere is possible).

Control over the applied downforce allows us to minimize the rolling resistance of the sphere and wear/attrition of both the sphere and the rolls. Note that when the sphere rotates in a direction parallel to the roll's rotation axis, the sensor provides no useful information (as the angular velocity component in this direction is equal to zero) and the roll's surface would simply grind on the surface of the sphere.

We discuss here a system concept rather than deliver a full description of a specific mechanical realization. Because first we have to analyze the designed system in a computational way to prove that our assumptions and equations are correct, and to analyze its behavior at the level of reflection, design, calculation and simulation. The system is very complex and expensive, therefore conducting the simulation study before the intended target experiment on a real system is highly recommended (underequipped experimenting with a human subject is unfounded). In this paper, we propose that the

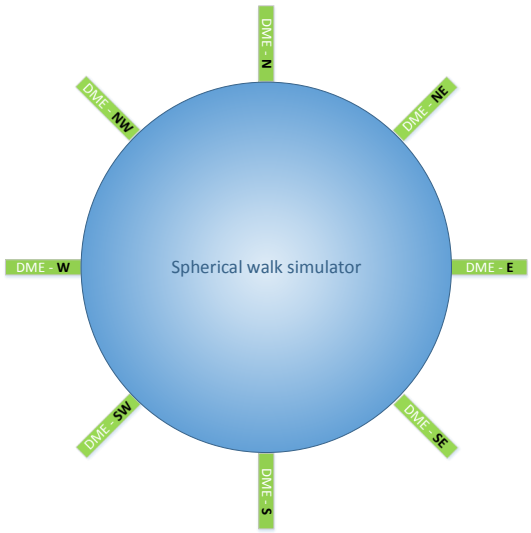

(a)

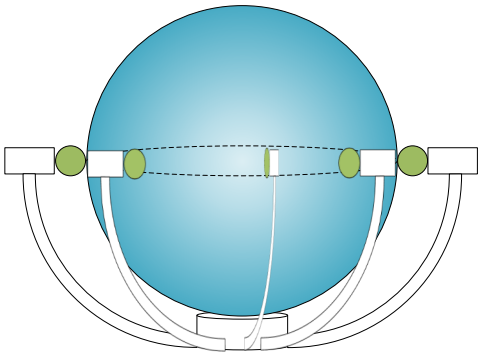

(b)

Fig. 2: Distribution of the DME drive and measurement elements around the sphere: (a) top view (b) side view.

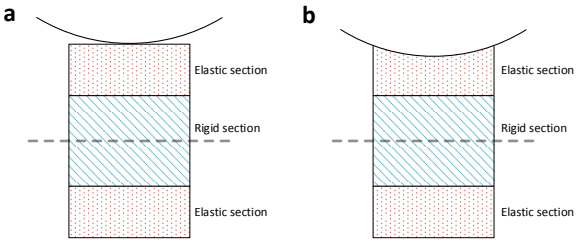

Fig. 3: Cross-section deformation of the roll, when downforce is: (a) minimal or (b) maximal.

downforce is controlled by a properly adjusted linear motor with feedback control. DME sphere driving can be achieved by an electric motor attached to each roll at the end of the linear motor. The roll speed can be measured using an optical shaft encoder, Hall-effect sensor, inductive sensor, etc. The force applied by the linear motor can be measured by a force

sensor integrated into the bearings, or by properly processed measurement of the current flowing through the motor.

The weight of the sphere is supported by omni-directional wheels, installed in the base of the mechanism. In the previous version of the system, there were supporting bars in the lower part of the sphere, which are now longer and supporting the DME elements (see Fig. II). Note however that in this paper we separate the problem of supporting the construction from the control issue, focusing on the latter.

III. Assumptions and Identified Issues of Modeling

The whole sphere-and-rolls system (SRS) can be approximately treated as a set of friction gears. There are two drawbacks of such gears [20]: low efficiency and microslips, which explain why such gears are not commonly used in engineering and control systems. Great attention has thus to be paid to modeling of such effects in order to minimize their impact on the overall system performance. The first problem is connected with measurement efficiency and grinding of the DME surfaces. The closer to 0° the (working) angle between the sphere rotation direction and the roll rotation axis, the lower the velocity component (more precisely, by the sine of this angle) measured by the sensor. Research is needed to determine the amount of energy wasted for frictional forces as a function of the angle between the roll and the sphere rotation direction (in an extreme case, when this angle is equal to 0°, the whole energy is being dissipated and DME provides no information about the velocity). On this basis, a function of downforce dependent on the working angle between the sphere rotation direction and the sensor position can be found. The aforementioned issue is connected with the rolls working as sensors (in PM). When the rolls affect the sphere's motion (in AM), the downforce applied, and thus the friction between the roll and the sphere, must be sufficient to efficiently transfer the torque from the driving roll to the sphere.

Another issue is connected with deviation of the point moving without slipping from the center of the contact area (CCA) - the geometric center of the figure formed by the sphere's and the roll's surfaces pressing against each other. This can be explained by the fact that the sphere can be seen as made of circles (being cross-sections of the sphere), and each of them is rotating with the linear velocity of the walker proportional to the cosine of angle θ - the angle between the direction of the walker's movement (also referred to as the rotation direction of the sphere's main cross-section, SMC) and a given DME cross-section (Fig. 4). This contributes to a distribution of linear velocities along the horizontal circumference of the sphere. Simultaneously, due to the non-zero width of the roll, it interacts in a certain range of angles, denoted by 2α in Fig. 4. This leads to another distribution of linear velocities along the roll's surface than in the case of the sphere. The location of the points on the CARS area (represented by the distance from CCA) moving with the same linear velocity, nonlinearly depends on angle β. These points will be called coincidence points (CP). Knowledge about the localization of these points is substantial, and will be used to link together the angular velocities of the rolls and the sphere. This issue is referred to as microslip.

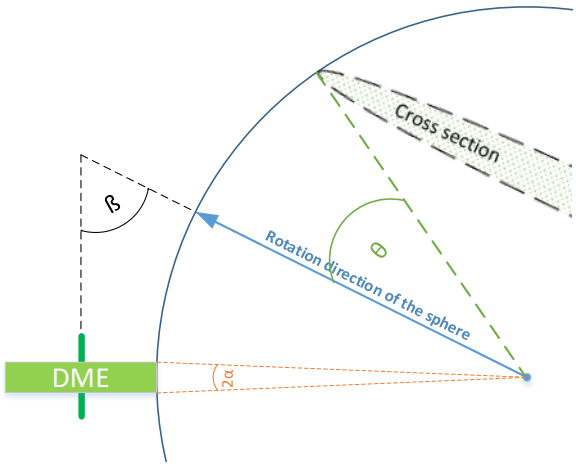

Fig. 4: Plan of the movement of the walker and a roll of DME, where β is the working angle between the rotation plane (and direction) of the SMC (blue arrow) and the rotation axis of the roll, and 2α is the angle which spans the CARS. θ is the angle between SMC and a cross-section of the sphere (top view).

Apart from the aforementioned difference between the distribution of linear velocities on a given roll and the sphere, some weights, resulting from the nonlinear distribution of downforce on the CARS area, have to be taken into consideration. Due to a possible rise in the probability of outlier occurrences in measurement when the downforce is small, a weight function, representing also the influence of measurements on dynamical state estimates of the sphere, has to be determined for particular DMEs. Such distribution can, for instance, assume the form of downforce function (versus angle β). As a result, the estimated velocity of the walker depends on the applied downforce, which also leads to different shapes of CARS (Fig. 5). Greater downforce increases the reliability of measurement. At the same time, however, the coincidence points (CPs) can recede from the CCA center. In a state estimation process, the impact of the downforce and the CP location on the estimated velocity has to be taken into account by using suitable weights.

In general, the issue of material wear is complex and depends on load force, speed, temperature, contact geometry, surface roughness, material and its elasticity etc. [22]. However, according to [23], [24], the wear rate of a material is proportional to the normal load. The force in a particular point of contact depends on material and its elasticity. Thus, we can associate the normal load with the downforce applied to each roll and measure the wear of its material as proportional to downforce (and by integration with respect to time, we obtain collective wear of the material in a certain time period). As suggested in [25], wear is proportional to the energy dissipated. By estimating the amount of dissipated energy, we can estimate the level of the material's wear. These relations will be used in the paper to assess the wear of the rolls during the system operation.

A specific downforce function has to be chosen to minimize the wear of the rolls and to minimize the amount of energy

dissipated on grinding, as well as to maintain high reliability of the measurement process.

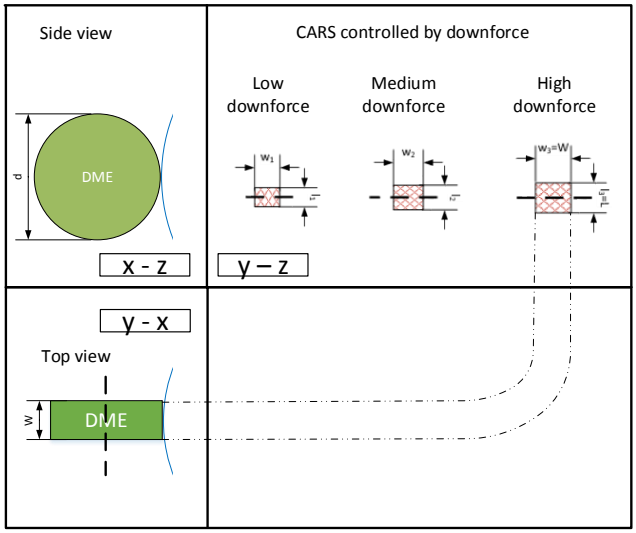

Fig. 5: Side and top views of the approximate shape of CARS - the contact area of the roll and the sphere (L - maximal length, d - diameter, W - maximal width) controlled by downforce.

A smooth-surface sphere (filled continuously, without holes necessary for the walker's comfort and breathing [1] - [3]) will first be considered with the assumption that the radius of the sphere is much greater than the radius of the roll. Thus, approximation of the sphere by a flat surface in a close proximity to each roll, is possible. Otherwise, simulation of the displacement effects can be conducted for a stationary roll using the finite element method, where CARS is bound to appear dependent on the downforce and the roll's material.

In further research an incomplete filling of the shell should also be considered, although it will lead to more complex models of DME's velocity w.r.t. the applied downforce and the rotation direction of the sphere.

For our current purposes, the rectangular CARS with a certain width W and length L induced by a fixed downforce (equivalent to the necessary geometrical displacement) has been assumed to roughly verify the importance of the addressed issues. For comparative purposes, two values of the friction factor f, 0.05 and 0.2, have been assumed. Recall that the radius of our laboratory sphere is 5 feet (1.52 meters).

IV. Analytic Relation Between Angular Velocity of the Roll and the Sphere

Considering forces acting on the roll and the sphere, we look for a relationship between the pertinent angular velocities. Amonton's law states that friction force (regardless of CARS) is related to downforce [21]. Thus the force cannot be an indicator of the rolls' attrition. However, the amount of energy dissipated on friction (heat and wear of the rolls) can be equivalent to the work performed by the sliding friction force. Assuming a constant friction factor f and a fixed contact surface area S, the mean friction force per unit area is

$$F_m = \frac{fP}{S} \tag{1}$$

where P is the downforce applied on the roll. Moreover, for simplicity, approximately uniform distribution of reaction forces over the contact area is assumed.

In order to compute the work done by friction forces in sliding fashion, the distance traveled by particular points of the roll relative to the sphere in time δt has to be estimated. The difference between the linear velocities of adjacent points on the roll and on the sphere, meaning the effective relative velocity associated with these points, will be denoted as $\Delta v(s)$, where s stands for a point's coordinate.

If $\Delta v(s) > 0$, then a braking friction force is acting on the roll, that is, a phenomenon called oversliding takes place (sliding of the roll on the sphere). In points, where the relative velocity is negative, an accelerating force is acting on the roll, that is, a phenomenon further called undersliding is observed. Points s, where $\Delta v(s) = 0$, corresponding to motion without sliding, will be referred to as the coincidence points (CP).

Discrepancy between the linear velocities on the sphere and the roll on the contact area for the working angle β=90°, is illustrated in Fig. 6. Fig. 7 shows the linear velocity distributions for two angles β=90° and β=45° with oversliding and undersliding indicated.

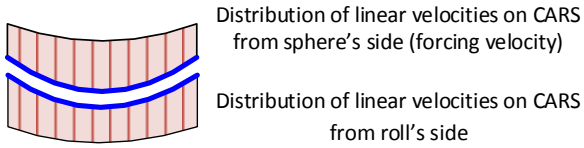

Fig. 6: Distribution of linear velocity over the contact area (CARS) for the working angle β=90°, and the sphere (the top part) excited by a moving walker and the roll (at the bottom) rotating at a constant speed (where blue lines denote the common contact area).

On the other hand, the common (constant) angular velocity of the roll for its working angle β needs to be found from the distribution of $\Delta v(s)$. The rotation speed can be determined as the one for which the work done by the braking and accelerating forces in time δt is in balance:

$$\int_S F_m \Delta v(s) \delta t ds = \int_S F_m \left(v_r(s) - v_s(s)\right) \delta t ds = 0 \tag{2}$$

where $v_r(s)$ is the linear velocity of the roll in point s and $v_s(s)$ is the linear velocity of the sphere in the same point. For the uniform distribution of the forces (1), it results that

$$\int_S v_r(s) ds = \int_S v_s(s) ds \tag{3}$$

Reducing the problem to one dimension (shown in Fig. 6), the friction forces need to be integrated solely along the width of the roll W (instead of the whole contact area, Fig. 5).

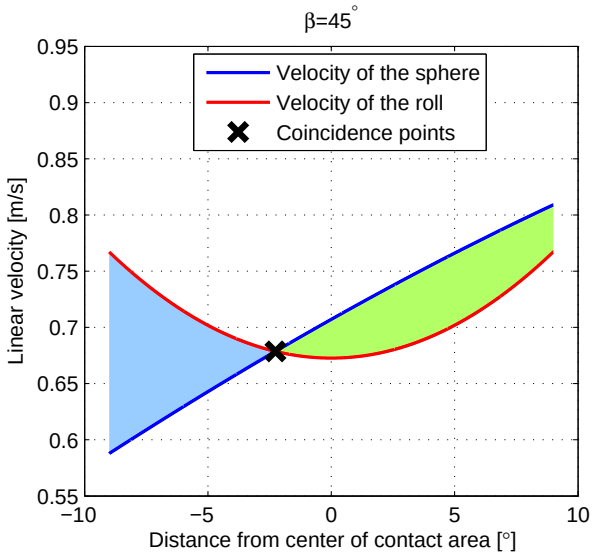

(a)

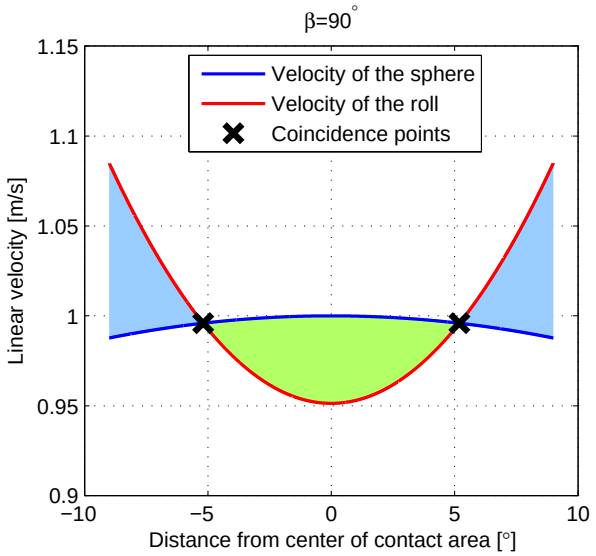

(b)

Fig. 7: Distributions of linear velocity over the contact area of the roll and the sphere for the working angles β equal to: (a) 45° and (b) 90° (blue color concern oversliding, while green - undersliding; the coincidence points are marked as crosses, and the angular width of the roll is 2α=18°).

By converting $v(s)$ into $v(\gamma)$, where γ is the angle within the contact area, the resulting equation representing energy balance acquires the form

$$\int_{\beta-\alpha}^{\beta+\alpha} v_r(\gamma)d\gamma = \int_{\beta-\alpha}^{\beta+\alpha} v_s(\gamma)d\gamma \tag{4}$$

The sought relationship between the angular velocities of the considered friction gear, can be obtained by equating these two integrals over the velocities of the sphere and the roll, respectively. Substituting the angular velocities for the linear ones: $v_r(\gamma)$=$\omega_r r(\gamma)$ for roll and $v_s(\gamma)$=$\omega_s R(\gamma)$ for the sphere, where ω_r is the sought angular velocity of the roll, ω_s is the known angular velocity of the sphere, $r(\gamma)$ is the radius of the roll's cross-section for a given angle γ, and $R(\gamma)$ is the radius of the sphere's cross-section for angle γ, one obtains:

$$\int_{\beta-\alpha}^{\beta+\alpha} \omega_r r(\gamma)d\gamma = \int_{\beta-\alpha}^{\beta+\alpha} \omega_s R(\gamma)d\gamma \tag{5}$$

A complete derivation of the angular velocity of the roll is provided in Appendix A. The resulting relationship is

$$\omega_r = \frac{-\omega_s\left(cos(\beta+\alpha) - cos(\beta-\alpha)\right)}{\left(\frac{r_0}{R_0} + cos(\alpha)\right)2\alpha - 2sin(\alpha)} \tag{6}$$

In order to confirm the validity of (6), numerical integration of (5) has been implemented taking into account the analytically obtained values (6) of ω_r. The computed difference between the left and right sides of (5) has proved to be close to zero (namely, $\sim 10^{-7}$).

V. Energy Dissipated on Friction

Once the angular velocity of the roll has been determined - minimization of the rolls' attrition can be approximately attributed to minimization of energy losses in the rotational motion of the sphere.

To calculate the work done by friction forces, we define the work as the product of force and corresponding displacement. For a given relative velocity $\Delta v(s)$ and time interval δt, we compute the resulting temporal displacement in space as $dx(s) = \Delta v(s)\delta t$. For equal treatment of the braking and accelerating forces, in calculation of the corresponding work done by friction forces, we use the absolute value of $\Delta v(s)$. Thus, the amount of energy dissipated in point s in time δt can be computed as

$$E(s,\delta t) = \int_S F_m|\Delta v(s)|\delta t ds \tag{7}$$

With the uniform distribution of friction forces over CARS and the rotational speed of the roll (6), from (7) the following energy dissipated on friction results:

$$E_{\delta t} = \int_{\beta-\alpha}^{\beta+\alpha} \frac{fP}{2\alpha}|\left(\omega_r\left(r_0 + R_0(cos(\alpha) - cos(\beta-\gamma))\right) + \right. \\ \left. -\omega_s R_0 sin(\gamma)\right)|\delta t d\gamma \tag{8}$$

which leads to

$$E_{\delta t} = \frac{fPR_0\delta t}{2\alpha}\int_{\beta-\alpha}^{\beta+\alpha}|\left(\omega_r\left(\frac{r_0}{R_0} + cos(\alpha) - cos(\beta-\gamma)\right) + \right. \\ \left. -\omega_s sin(\gamma)\right)|d\gamma \tag{9}$$

Equation (9) has been implemented numerically to determine the work performed by friction forces. Fig. 8 shows the

temporal energy dissipated on friction in each time interval δt=1 second with downforce P=100 newtons versus the working angle β for two different friction factors.

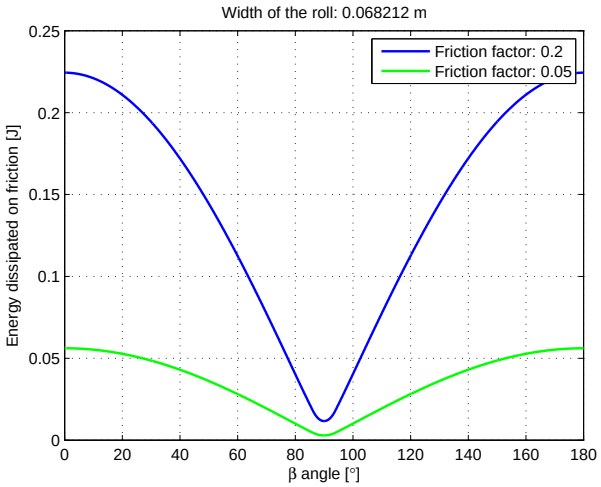

Fig. 8: Temporal energy dissipated on friction versus roll's working angle β with friction f=0.05 and f=0.2, and downforce P=100 newtons.

It becomes clear from Fig. 8 that the lowest energy loss for a single roll occurs at β=90° (walk towards this roll), and is almost twenty times lower than the maximal losses appearing at the angle 0°. To reduce the amount of dissipated energy, the downforce has to be minimized (preferably to 0) for angles closer to 0° and 180°. A graph presenting energy losses, when the downforce varies according to P=100 · sin(β) [newtons], and the contact area is assumed to be linearly dependent on downforce (see Fig. 5), is presented in Fig. 9, showing significantly lower losses. Note that here a two-fold action takes place. Due to a certain elasticity of the material, there exists a relationship between downforce and the contact area, because the downforce causes displacement, and the displacement determines the downforce required to achieve a given contact area. We assume that there is an identified function converting displacement to contact area and required downforce. In the conducted experiments, since (9) is reduced to a one-dimensional equation, the contact area is assumed to be linearly dependent on the applied downforce. Further research should consider nonuniform distribution of the forces along the contact area and finding an optimal relationship of the downforce and angle β assuring high reliability of the measurements as well as low energy losses.

VI. Estimation of the Roll's Angular Velocity

Estimation of the roll's angular velocity is substantial for determination of the walker's velocity and direction. In this paper, three methods of estimation are proposed: method of velocity analysis (MVA), method of partial masses (MPM), and method of surface mean velocity (MSM). A short comparison of the methods is presented in Tab. I.

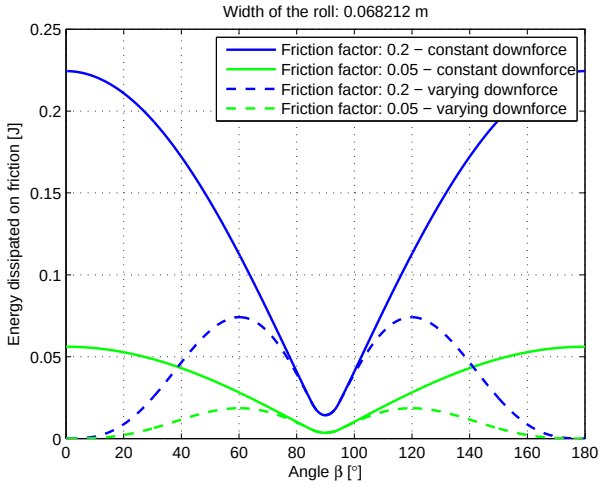

Fig. 9: Temporal energy dissipated on friction versus angle β for friction f=0.05 and f=0.2 under the constant downforce (continuous lines) and the varying downforce (dashed lines).

TABLE I: Three proposed methods for estimating the angular velocity of working rolls.

Name	Concept	Nature	Needs precise CP location?	Execution time*
MVA	Physical relation/ Energy conservation law	Analytic	Yes	4 μs
MPM	Division into smaller friction gears	Numeric	No	130 μs
MSM	Mean velocity of the sphere as the velocity in CP	Numeric	Yes	120 μs

* For uniform distribution of downforce.

A. Method of Velocity Analysis (MVA)

In the first approach, the angular velocity of the roll will be determined analytically from (6). The value obtained from this equation is the angular velocity of the roll, for which the work due to the effects of oversliding and undersliding are equal. The developed approach to computation of the roll velocity (6) will be referred to as the method of velocity analysis (MVA).

The MVA approach consists in finding the coincidence points (CPs) on the CARS area, which move without slipping. Numerical simulations have been conducted to determine the distance, denoted as λ, of the CPs (in degrees) from the CCA center. The results are presented in Fig. 10.

For a certain range of angles β (the shaded area in Fig. 10) close to 90°, two CPs exist on the contact area (see also Fig. 7). For β=90°, the two CPs ('*') are located symmetrically relative to CCA. When increasing the angle, one of the points moves to the edge of the roll (green line), and next disappears, while the second (red line) travels towards the CCA.

The location of CPs and the radii of the corresponding sphere's and roll's cross-sections are sufficient to find the relationship between their angular velocities, and, consecutively, to be used in estimating the walker's linear velocity.

Two other methods of (numeric) estimation, referred to as the method of partial masses (MPM) and the method of surface mean velocity (MSM), are proposed here for the maximum

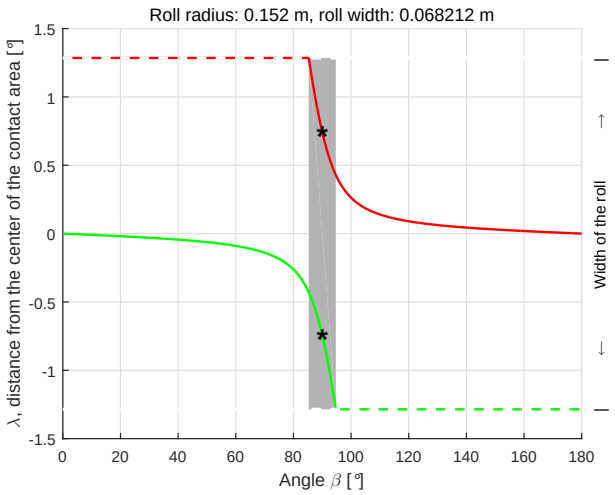

Fig. 10: Distance λ of the coincidence points from the center of the contact area CCA (dashed lines denote the points lying outside of the roll, shaded area represents the range of angles β with two coincidence points).

downforce case, and compared in a numerical study.

B. Method of Partial Masses (MPM)

Assuming a dense discretization of the roll into separate narrow sections (discs), the cross-sections of both the sphere and the roll can be seen as a set of undeformed friction gears. Fig. 11 presents two distinct gears: (1) a gear drive made of discs of radii R_1 (describing the main cross-section of the sphere) and r_1 (representing a disc cross-section of the roll), and (2) a similar gear drive modeled by radii R_2 and r_2.

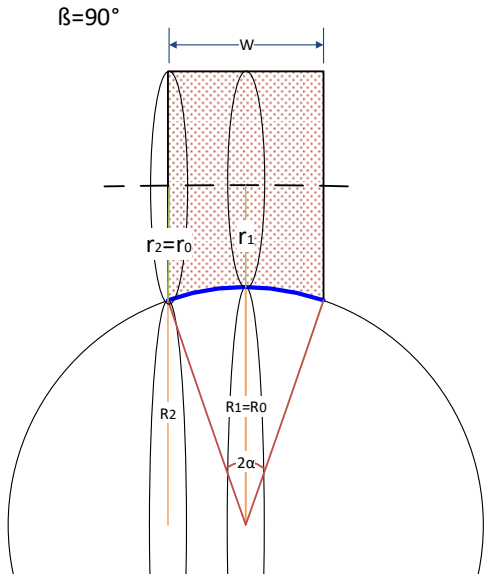

Fig. 11: CARS (blue line) and the corresponding cross-sections for β=90°.

The ratio of angular velocities for the considered friction gear drive as a function of angle γ (within the active range of 2α) equals the inverse ratio of the corresponding radii:

$$\frac{\omega_r(\gamma)}{\omega_s} = \frac{R(\gamma)}{r(\gamma)} \tag{10}$$

where ω_r is the angular velocity of the roll, ω_s denotes the angular velocity of the sphere, R - the radius of the sphere for a given contact point, r - the radius of the roll for this point. Note that the angular velocity of the sphere, forcing the drive, remains constant for each cross-section. For a given linear velocity $V(\gamma)$ of the points at the sphere, the corresponding angular velocity of the roll is

$$\omega_r(\gamma) = \frac{V(\gamma)}{r(\gamma)} \tag{11}$$

Scaled integration along the contact area lead us to the computation of the mean angular velocity, $\bar{\omega}_r$, of the roll:

$$\bar{\omega}_r = \frac{1}{2\alpha} \int_{\beta-\alpha}^{\beta+\alpha} \frac{V(\gamma)}{r(\gamma)} d\gamma \tag{12}$$

By the known relationship for linear velocities $V(\gamma)$=$V_p sin(\gamma)$=$\omega_s R_0 sin(\gamma)$, where V_p is the velocity of the walker, and $r(\gamma) = r_0 + R_0(cos(\alpha) - cos(\beta - \gamma))$ (see Appendix B), the following formula is obtained:

$$\bar{\omega}_r = \frac{1}{2\alpha} \int_{\beta-\alpha}^{\beta+\alpha} \frac{V_p sin(\gamma)}{r_0 + R_0(cos(\alpha) - cos(\beta - \gamma))} d\gamma \tag{13}$$

where r_0 and R_0 are the maximal radii of the rolls and the sphere, respectively, which results in

$$\bar{\omega}_r = \frac{\omega_s}{2\alpha} \int_{\beta-\alpha}^{\beta+\alpha} \frac{sin(\gamma)}{\frac{r_0}{R_0} + cos(\alpha) - cos(\beta - \gamma)} d\gamma \tag{14}$$

Nonuniform distribution of the friction forces on CARS can be modeled by some weight $w(\gamma, l)$, representing a relative impact of particular velocities on the result. Symbol l stands for the second dimension of the contact area (dependent on downforce the actual length $L_a \in [\delta l, L]$, where $\delta l > 0; \delta l \approx 0$, and L is maximum length). Then

$$\bar{\omega}_r = \frac{\omega_s}{2L_a\alpha} \int_{\beta-\alpha}^{\beta+\alpha} \int_{-L_a/2}^{L_a/2} \frac{w(\gamma, l) sin(\gamma)}{\frac{r_0}{R_0} + cos(\alpha) - cos(\beta - \gamma)} dl d\gamma \tag{15}$$

Substituting a corresponding width w for angle γ we have

$$\bar{\omega}_r = \frac{\omega_s}{WL_a} \int_{-W/2}^{W/2} \int_{-L_a/2}^{L_a/2} \frac{w(x, l) sin(\gamma(x))}{\frac{r_0}{R_0} + cos(\alpha) - cos(\beta - \gamma(x))} dl dw \tag{16}$$

The above method of estimating the angular velocity of the roll will be called the method of partial masses (MPM). Note

that this method does not require the knowledge about the location of CPs.

C. Method of Surface Mean Velocity (MSM)

Similar reasoning can be applied when one considers sliding on the contact area, resulting from nonuniform distribution of linear velocities along the contact area. The mean linear velocity of the sphere can be obtained as

$$\bar{V_s} = \frac{1}{2\alpha} \int_{\beta-\alpha}^{\beta+\alpha} V(\gamma) d\gamma \tag{17}$$

Assuming that the mean velocity of the sphere is close to the one in CP (for computed $\bar{V_s}$ and CP/location), the relationship between the angular velocities of the roll and the sphere can be found based on the radius of the roll in the CP point r_λ (or weighted mean of the results in the case of multiple CPs). Thus the sought estimate of the angular velocity of the roll is

$$\hat{\omega}_r = \frac{\bar{V_s}}{r_\lambda} \tag{18}$$

The above estimate of the angular velocity of the roll will be referred to as the method of surface mean velocity (MSM). However, when considering different values of friction forces on CARS through weights $w(\gamma, l)$, representing local down-force in particular points, the mean surface velocity can be obtained as

$$\bar{V_s} = \frac{1}{2L_a\alpha} \int_{\beta-\alpha}^{\beta+\alpha} \int_{-L_a/2}^{L_a/2} V(\gamma) w(\gamma, l) dl d\gamma \tag{19}$$

D. Comparative Study

Assuming unitary weights and a constant speed of the walker, the estimated results of the two numerical methods have been obtained by performing numerical integration in (14) and (17). However, since the MSM estimation concerns linear velocity, it should be converted by (18) to the common estimated quantity for MPM and MSM, i.e. the angular velocity. In the full-blown, two-dimensional case, (15) and (19)-(18) should be respectively used. However, with the applied unitary weights, and based on the averaging feature of the integrals in (15) and (19), the problem reduces to one dimension (without going into technical details, for every $L_a \in [\delta l, L]$, integration along the roll's length is symmetrical and – due to the unitary weighting – ineffective). Most important are estimation results in proximity of β=90° (due to the fact that the roll gives there the highest amount of information about the walker's motion). The effects of the methods are shown in Fig. 12, when the ratio of the roll's and sphere's radii equals 0.1 and the width of the roll equals 6.8 cm.

The divergence of the velocities obtained via the methods MPM and MSM with reference to the MVA estimate is illustrated in Fig. 13.

In the considered case both numerical methods, MPM and MSM, can be used for estimating the angular velocity of

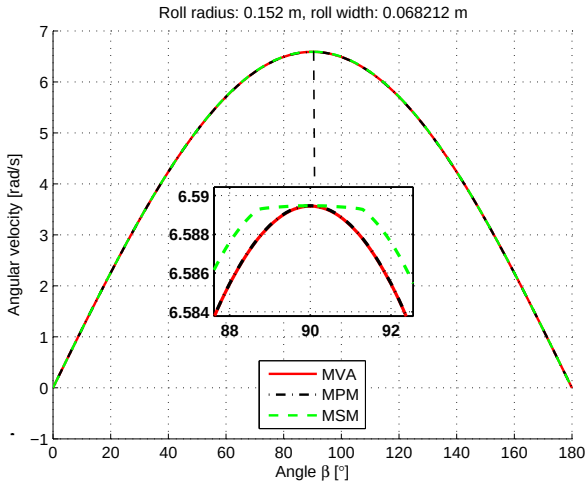

Fig. 12: Three estimators of the angular velocity of the roll versus the working angle β (ratio of the roll and the sphere radii is 0.1 and the width of the roll is 6.8 cm).

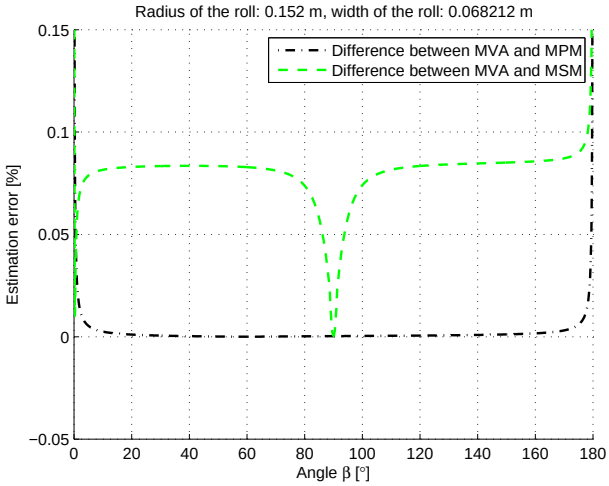

Fig. 13: Relative absolute value of the difference between the velocity estimations obtained from MVA and the ones resulting from MPM and MSM, where normalization has been performed w.r.t. the MVA values (the ratio of the roll to the sphere radii is 0.1, and the width of the roll is 6.8 cm).

the rolls with satisfactory accuracy. Note however that a 1% estimation error can be achieved when the radius of the roll is at least about 120 times smaller than the radius of the sphere, when the roll width (Fig. 12) equals 0.04 radius of the sphere. The same level of estimation precision (1%) can be obtained when the roll width is greater than at least about 0.15 radius of the sphere, for the roll radius equal to 0.1 radius of the sphere. The above numbers are though exemplary, as the estimation error function has two arguments, and depends both on the width and the radius of the roll. Nevertheless, when the radius of the roll is too small as compared to the radius of the sphere, or when the roll is too wide, the results obtained by the two methods MPM and MSM can significantly differ from their reference values of MVA. To visualize the problem better, the

simulated width of the roll has been raised to 47.5 cm. The obtained velocity distributions are presented in Fig. 14 and the corresponding relative estimation errors are shown in Fig. 15.

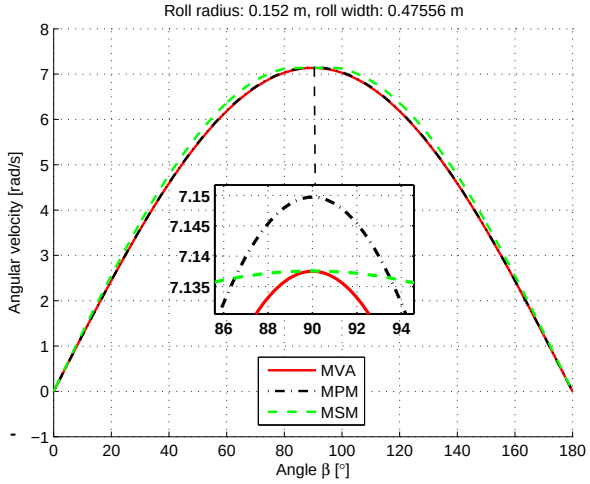

Fig. 14: Numerical estimators of the angular velocity of the roll versus the working angle β (ratio of the roll and the sphere radii is 0.1 and the width of the roll is 47.5 cm).

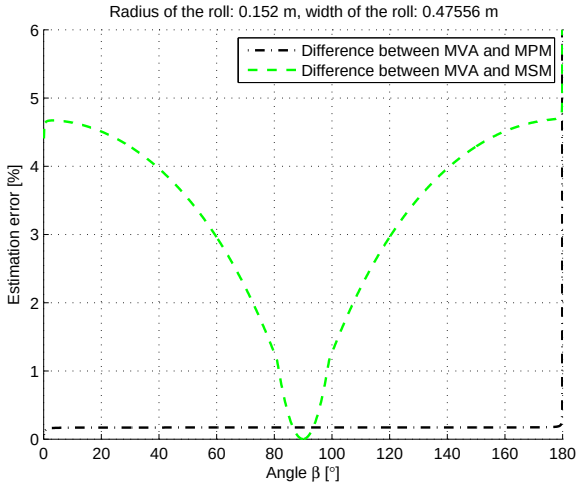

Fig. 15: Relative absolute value of the difference between the velocity estimations obtained from MVA and the ones resulting from MPM and MSM (normalization done against the MVA values, and the ratio of the roll's to sphere's radii is 0.1, and the width of the roll is 47.5 cm).

As shown in Fig. 15, in a small neighborhood of β=90°, the error of MSM is slightly lower than the error of MPM. However, even a slight deviation from this angle makes MPM a better estimator of the angular velocity.

With the radius of the roll much smaller than the radius of the sphere, the computed angular velocities are shown in Fig. 16, and the corresponding relative estimation errors are presented in Fig. 17.

For a significantly small ratio of the radii of the roll and the sphere, and as compared to MPM, MSM is a better estimator in a wider proximity of β=90°. In the proximity of 0° both

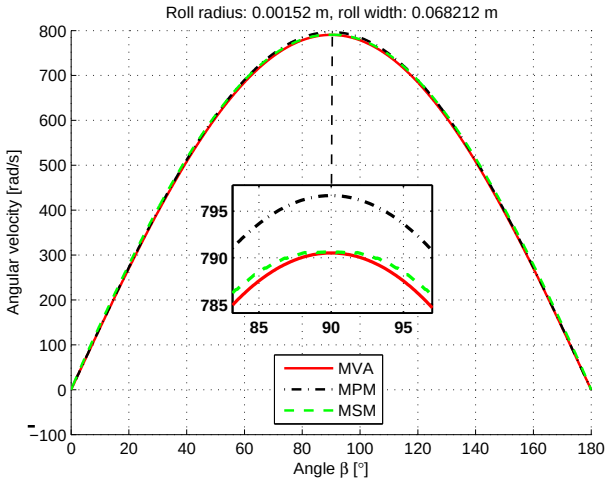

Fig. 16: Three estimations of the angular velocity of the roll versus angle β (ratio of the roll and the sphere radii is 0.001 and the width of the roll is 6.8 cm).

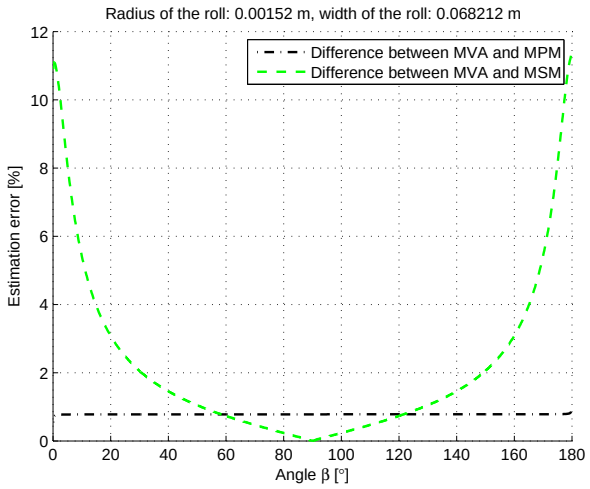

Fig. 17: Relative absolute value of the difference between the velocity estimations obtained from MVA and the ones resulting from MPM and MSM (normalization by the MVA value; the ratio of the roll to the sphere radii is 0.001, and the width of the roll is 6.8 cm).

estimators correctly tend to zero (though the relative error of MSM and MPM goes to infinity), which is even more effective with downforce and weighting approaching zero in the neighborhood of β=0°.

The error of MPM slightly increases when decreasing the ratio of the roll's to the sphere's radius, which may result from the higher angular velocities of the rolls. The MSM estimation error is greater for wider rolls in a wider range of angles than in the case of narrow rolls. The cause of this effect lies in averaging a higher range of angles, and as a result, the estimate of the non-sliding velocity is less accurate.

Both numerical methods are thus suitable for estimating the angular velocity of DMEs. In the simple case of uniform distribution of the applied downforce, the execution time of the

analytical method MVA is much shorter than that necessary for the numerical approaches MSM and MPM (see Tab. I). Nevertheless, in other practical cases one should benefit from the direct feasibility of the proposed numerical methods. On the other hand, from the fact that the three presented methods provide consistent results (for appropriate, analytically and technically/physically convenient dimensions of the sphere and rolls), we conclude that the presented design approach is correct.

VII. Rotational Motion Estimation (RME)

The above results can be utilized for estimating the velocity and the rotation direction of the sphere, translating measured rotational velocities of the rolls to estimates describing rotational motion of the sphere. The proposed procedure, further referred to as rotational motion estimation algorithm (RME), will be presented in a few phases.

During an initialization phase of this algorithm, all measurements are treated equally, i.e. each measurement has the same confidence level (represented by equal weights). Thus, the initial results (the angular velocity and rotation direction of the sphere) are estimated based on all possible measurements.

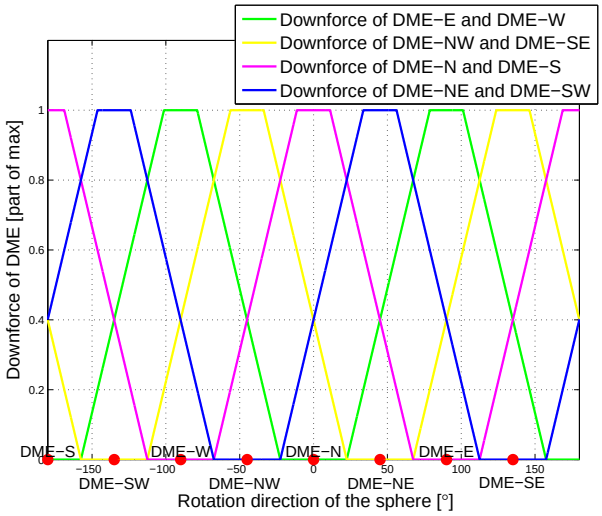

Fig. 18: Distribution of downforce for particular DMEs versus the rotation direction of the sphere.

The estimation (6) of the angular velocity of the roll allows us to compute the velocities of the rotating rolls, when the angle between the rotation plane of the sphere and the rotation axis of the roll is β, the width of the roll translates into its angular spread 2α, the radius of the undeformed roll is r_0, the radius of the sphere is R_0, and the sphere is rotating with angular velocity ω_s. Moreover, the simplifying assumption about the uniform distribution of forces on CARS is taken. The material of the roll has to be selected in such a way that the roll remains undeformed on the edges (the circular bottom sides of the roll) when full downforce is applied.

However, usually the aim is to determine the angular velocity of the sphere and the linear velocity of the walker, knowing the measured angular velocity of the roll. Thus function (6) has to be inverted to obtain

$$\omega_s = \frac{-\omega_r \left(\left(\frac{r_0}{R_0} + cos(\alpha) \right) 2\alpha - 2sin(\alpha) \right)}{(cos(\beta+\alpha) - cos(\beta-\alpha))} \tag{20}$$

The relation between the linear velocity of the walker v_w and the linear velocity measured by a given roll v_r is

$$v_w = \frac{v_r}{sin(\beta)} \tag{21}$$

where β is the angle between the rotation direction of the sphere and the rotation axis of the roll. The measured velocity v_r is assumed to be known from one of the methods presented in the previous section. However, the working angle β is unknown. To identify β, at least two measurements are necessary. Let v_r^i, where $i = 0, 1, 2, ..., 7$, be the linear velocity measured by DME of the number i, where $i = 0$ means DME-N (DME heading north), $i = 1$ - DME-NE (DME heading north-east) and so on (see Fig. 2a). For each measurement and the sphere's radius R, the following relation holds:

$$v_r^i = Rsin(\beta^i) \tag{22}$$

For two neighboring sensors $(i,\ i+1)$, the following angle relation is fulfilled: $\beta^{i+1} = \beta^i + \frac{\pi}{4}$, so one can state that

$$\frac{sin(\beta^i + \frac{\pi}{4})}{sin(\beta^i)} = \frac{v_r^{i+1}}{v_r^i} \tag{23}$$

which, by the well-known identity $sin(a+b) = sin(a)cos(b) + cos(a)sin(b)$, leads to

$$\frac{sin(\beta^i)cos(\frac{\pi}{4}) + cos(\beta^i)sin(\frac{\pi}{4})}{sin(\beta^i)} = \frac{v_r^{i+1}}{v_r^i} \tag{24}$$

By rearranging (24), the angle β^i can be estimated as

$$\beta^i = actg\left(\frac{\sqrt{2}v_r^{i+1}}{v_r^i} - 1 \right) \tag{25}$$

Using (25) in (21), the speed of the walker estimated by the i-th DME (v_r^i), when v_r^{i+1} is known, can be computed as

$$\hat{v}_w(i|i+1) = \frac{v_r^i}{sin\left(actg\left(\frac{\sqrt{2}v_r^{i+1}}{v_r^i} - 1 \right) \right)} \tag{26}$$

Similarly, the velocity of the walker estimated by the i-th DME, with the knowledge of v_r^i and v_r^{i-1}, can be judged as

$$\hat{v}_w(i|i-1) = \frac{v_r^i}{sin\left(actg\left(1 - \frac{\sqrt{2}v_r^{i-1}}{v_r^i} \right) \right)} \tag{27}$$

Equations (26) and (27) can be applied for each DME (certainly, all the measurements used in calculations have to be non-zero). In such a way, a set of velocity estimates can be built. Note that the estimators working on the opposite side of the sphere (with respect to the direction of the walk), give opposite (negative) signs of the estimated angular velocities. Thus, for the final estimation of the walker's velocity, the absolute values of the partial estimates have to be taken into account. The estimate $\hat{v}_w$ is derived as a properly weighted superposition of the partial estimates.

Once the estimate of the walker velocity $\hat{v}_w$ is known, an estimate of the rotation angle $\hat{\psi}$ (related to the positive axis y, heading north) can be obtained from:

$$\hat{\psi}^i = sign(i)acos\left(\frac{v_r^i}{\hat{v}_w^i}\right) + \delta^i \tag{28}$$

where $sign(i)$ is a function defined as:

$$sign(i) = \begin{cases} -1, & \text{if } \hat{v}_r^{i-1} > \hat{v}_r^{i+1} \\ 1, & \text{if otherwise} \end{cases} \tag{29}$$

and δ^i is the angle of i-th DME related to the positive y axis (north). Again, only non-zero velocity estimates should be considered in the collected set of estimates. The final estimate $\hat{\psi}$ is derived via a properly weighted superposition of (28).

On the basis of the estimated rotation angle, suitable regulation of downforce can be put into practice according to assumed distribution characteristics presented in Fig. 18. This distribution has been applied intuitively, and seems to result in a good compromise between the dissipated energy and the range of angles for which DME measurement is informative (lower downforce can easily cause additional outliers in the measurements). Certainly, this issue creates an optimization problem, in which the dependency between the downforce and the probability of outliers occurrence is also needed.

In consecutive measurement steps we assign weights to each DME associated with its measurement reliability, which are linearly proportional to this distribution (and nonlinearly dependent on the working angle between the roll's rotation axis and the rotation direction of the sphere). Such weights determine the effective input of particular measurements on both the estimated velocity and rotation direction of the sphere, in the next time step.

When the downforce and measurement weights of particular rolls are fixed, the system can properly estimate the velocity and the rotation direction of the sphere. Afterwards, the mode of the system can be changed to active. Then, based on the obtained estimates, the control signals for each DME are generated, by a properly tuned algorithm. In such a way the system is able to force the walker movements at a specified speed, direction of the sphere rotation (via properly calculated turn velocities of the DMEs), and to control the sphere's inertia during walker's movement. Certainly, the downforce used in the active mode should be increased to efficiently affect the sphere by the driving rolls.

After downforce actuation of DMEs, the system continues measurement in passive mode and repeats subsequent steps (omitting the initialization phase). A diagram of the RME algorithm for active walk is presented in Fig. 19.

A. Testing the RME Algorithm

Simulations were conducted to validate the effectiveness and applicability of the proposed RME algorithm. A simple trajectory of the walker's movement was simulated: first, straight walk with constant acceleration, and next rotation at a fixed rate and velocity. This trajectory is presented in Fig. 20, whereas the linear velocity and the direction of the walker's movement versus time are presented in Fig. 21.

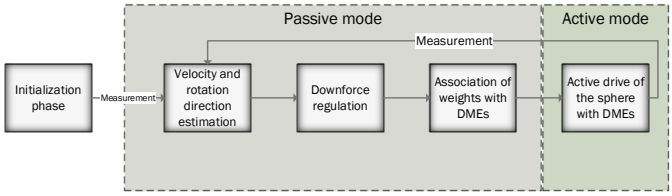

Fig. 19: Control of the intelligent sphere during active walk in passive and active modes.

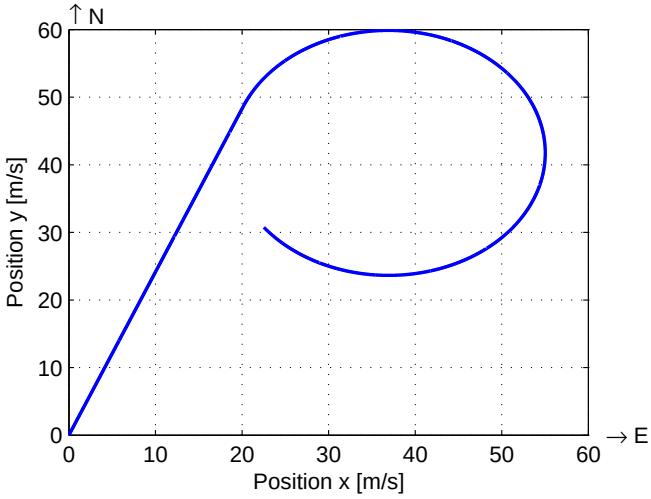

Fig. 20: Simulated trajectory of the walker's movement.

For the experiment of Figs. 20 and 21, the velocities measured by four DMEs and the calculated downforce are shown in Figs. 22 - 25.

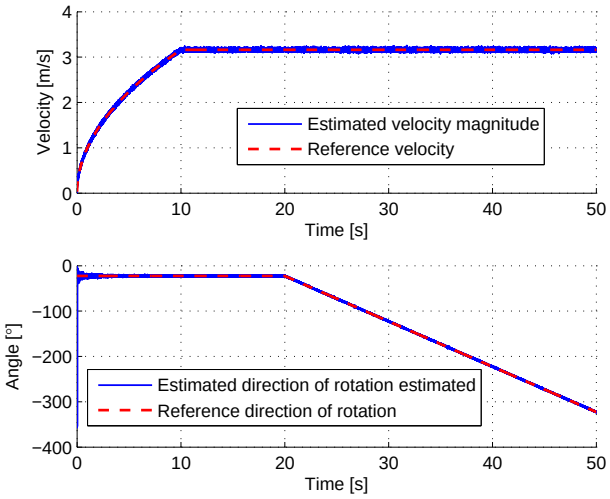

Fig. 21: Linear velocity and direction of the walker's movement simulated (red) and estimated (blue).

In presence of zero-mean gaussian measurement noise and the respective signal-to-noise ratio $SNR = 30dB$, the velocity estimated by the RME algorithm and its estimates of the turning direction, very well approximate the reference ones.

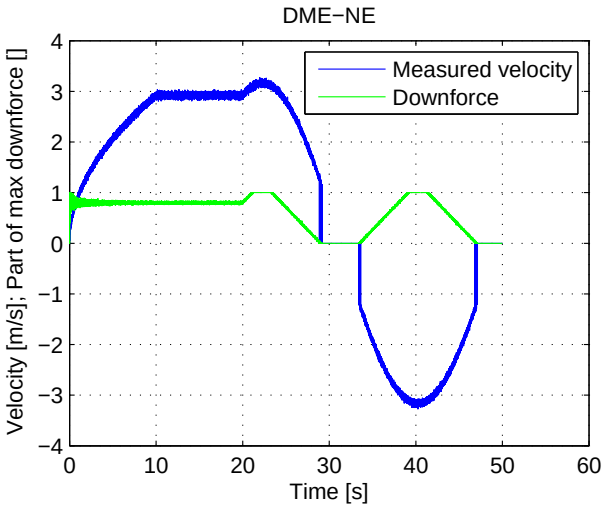

Fig. 22: Velocities measured by DME-NE (blue) and downforce (green) for DME calculated by the RME algorithm.

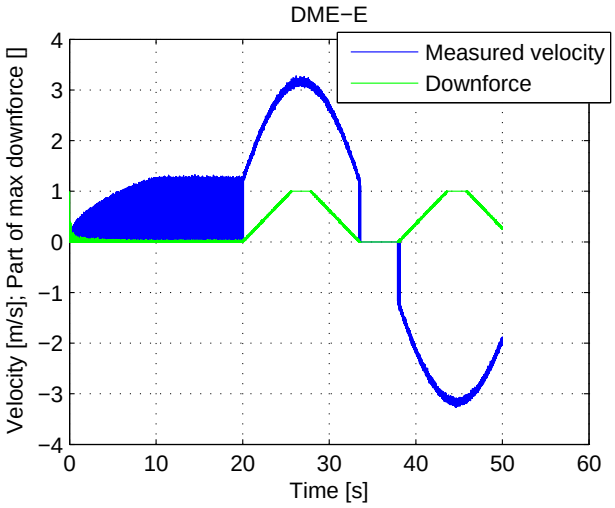

Fig. 23: Velocities measured by DME-E (blue) and downforce (green) for DME calculated by the RME algorithm.

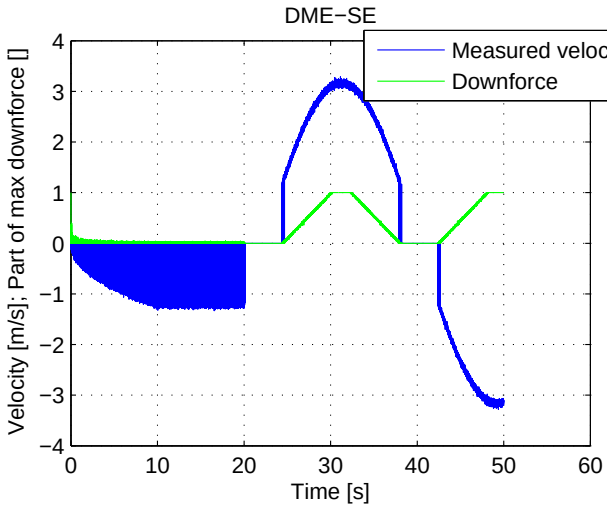

Fig. 24: Velocities measured by DME-SE (blue) and downforce (green) for DME calculated by the RME algorithm.

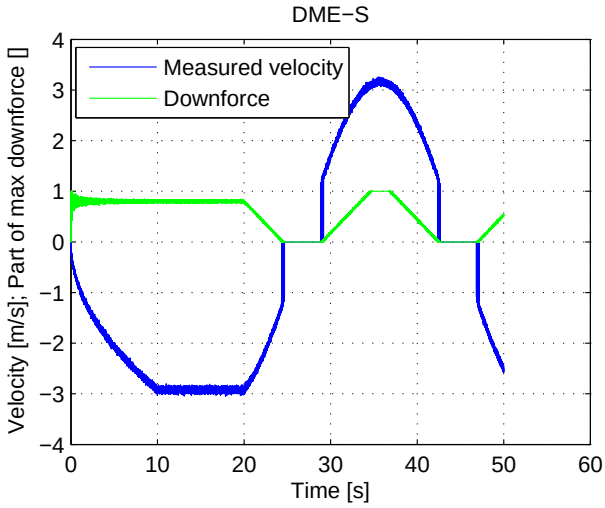

Fig. 25: Velocities measured by DME-S (blue) and downforce (green) for DME calculated by the RME algorithm.

Several initial estimates appear to differ from their reference values, but next, the RME algorithm stabilizes around the true value in a few steps. A foreseeable effect occurs in the beginning phase, when two DMEs (E and SE, those almost perpendicular to the direction of walk) are toggled on and off. The dark blue areas in Figs. 23 and 24 indicate the initial measurement uncertainty that causes the phenomenon of alternating clamping and detaching of the roll from the sphere. Despite such commutations, the RME algorithm is able to correctly estimate the velocity and the direction.

B. Limitation of the Algorithm

The limitation of the presented method is mainly related to the precision of angular velocity measurements. Despite the fact that we do not provide here any specific instrumentation, the target design must be prepared with due regard to the limitations. One way to measure angular velocity is to use a Hall-effect sensor or optical shaft encoder; however such measurements are limited by the accuracy of the encoder. Another option is to measure the current frequency on the alternator windings connected to the shaft of the cylinder. Accuracy is then limited by the measuring equipment and the gear used. In addition, the alternator during measurement can generate a breaking force on the roll and disturb the measurement.

Nevertheless, the performed numerical study shows that the RME algorithm is able to track the walker's trajectory on a satisfactory level even when the measurements are corrupted by a Gaussian noise process.

C. Further Research

In further technical research the displacement of the roll ought to be determined as a function of downforce and the degree of sphere filling, and of other mechanical properties of the material used. For such research, the finite elements method appears to be most suitable. It could even lead to more

precise determination of CARS, and thus to better estimates of the angular roll's velocities. The friction factor necessary for our calculations can be effectively estimated using a haptic methodology [26].

Nonuniform distribution of the reaction forces on the contact area should also be considered, and the deformation of this distribution occurring during operation of the rolls. Such an effect, for a cylinder rotating on a flat surface, is presented in Fig. 26. Certainly, the final accuracy of the RME algorithm should be tested in field trials.

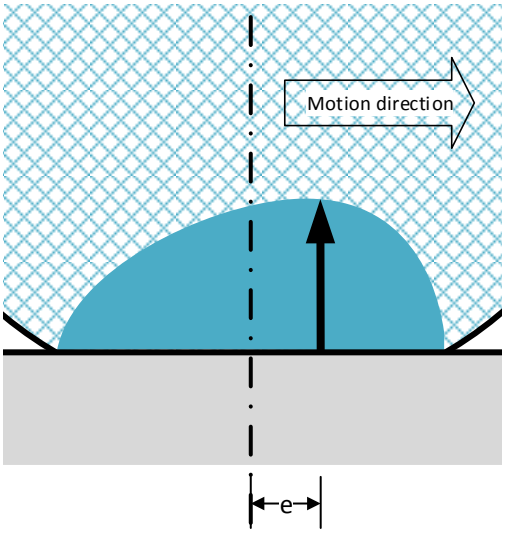

Fig. 26: Nonuniform distribution of the reaction forces on the contact area for the second dimension (symbol e denotes the shift of the maximum reaction force with regard to the center of the contact area [29]).

VIII. Conclusions

An active drive-and-measurement system for haptic interaction with physical and augmented reality has been proposed in this paper. The system consists of the DME elements distributed around the sphere in fixed positions, every 45°. A single DME is made of a linear actuator with force feedback, at the end of which the electric motor is attached and coupled with the roll. The linear actuator controls the downforce applied to the roll, pushing it against the sphere. The electric motor is driving the roll. The angular velocity of the roll is measured. One control loop regulates the downforce, according to the described algorithm (where downforce is dependent on the relative angle between DME and the rotation direction of the sphere). The second control loop deals with the angular velocity of the roll in Active Mode, according to the preprogrammed path to be followed by the walker. In Passive Mode, the angular velocity of the roll is measured, which is further processed by the proposed Rotational Motion Estimation algorithm.

Two issues has been addressed: the existence of microslips reflected in deviation of the coincidence points from the center of the contact area, linking together the angular velocities of the roll and the sphere, and low efficiency reflected in the attrition of the rolls. The analysis of the system has been performed showing the practical relation between the angular velocities of the sphere and the roll. Moreover, the benefit from utilizing adjustable downforce has been shown, which leads to minimization of the energy losses, and as a result, to minimization of the wear of the rolls.

Although the issue of measuring the wear of material is rather complex, and depends on many parameters, our solution relies on dependencies between the wear of material and applied load or dissipated energy (both approaches are consistent). Simply speaking, through properly adjusted downforce, we optimize the wear of the material by minimizing the energy dissipated by friction. Another problem is related to the production of the desired resistance. Designing friction gears is considered problematic in the field of mechanics. This paper proposes a well-thought-out solution based on several physical relationships, including Amonton's law stating that friction force is independent of the contact area but proportional to the downforce.

We also took a deeper insight into the physics behind the friction gears interaction. Note that for reasonable physical parameters of the system all the methods are consistent and yield similar results (see Fig. 13). Through the analysis of physical dependencies during the contact of the roll and sphere, using energy conservation principle, we have determined the relative velocities, for which the energy is in equilibrium. In addition, we have shown an interesting relationship (9) between dissipated energy and applied downforce. Importance of control over downforce is illustrated by Fig. 9. Moreover, when providing the algorithm for estimating the walker's position, we assume an intelligent distribution of the downforce applied to DMEs, according to the given angle of motion (see Fig. 18). This distribution has been applied intuitively, and seems to give a good compromise between the energy dissipated on friction and the range of angles for which DME measurement is informative (lower downforce can easily cause additional outliers in the measurements).

In further research, nonuniform distribution of the reaction forces on the contact area, and a not completely-filled sphere, should be considered.

Moreover, the problem of numerical estimation of the angular velocity of DME has been addressed. Two approaches, a method of partial masses and a method of surface mean velocity, have been proposed. Efficiency of these methods has been investigated, taking into account the physical dimensions of the system's components. With the assumptions proposed in this work, the numerical results coincide with the analytical computations. It has been interesting to see that as compared to the analytic formula, both numerical methods can be used to approximately estimate the angular velocity of a working roll.

A master (RME) algorithm for estimating the rotational motion parameters has also been proposed. The derivation of the RME procedure has been described in detail and the resulting estimator of the velocity and direction of a walker inside the sphere have been provided. In this approach, we have applied a downforce function empirically adjusted, although more profound research could be done on this issue, which can

be defined as a multi-parameter optimization problem. Instead, we have proposed reducing the impact of potentially corrupted measurements by introducing a simple weighing mechanism into the estimation algorithm.

The problem with choosing the method of measuring the angular velocity of rolls have also been hinted, which can be solved by including Hall-effect sensors, optical encoders, inductive sensor, or measuring the current induced by a rotating roll (e.g. in an alternator). The force produced by the linear motor can be measured for instance by a force sensor integrated with the bearings or by properly processed measurement of the current flowing through the motor.

The accuracy of the above design propositions should certainly be confronted with maximum allowable errors. Though very important, such deliberations are not simple in practice. Nevertheless, they should be thoroughly carried out during the mechanical-and-electrical design of the target system, after the presented validation performed by computation and simulation.

As an extension of the current design based on the originally designed DME elements, the proposed concept can be used to build integrated haptic systems for remote control of mobile robots that can be used in tourism or culture, or for training or instructing police, military, or firefighters.

Referring to the current state of development of the system, where we have only a mechanical construction of the sphere, without a measuring system and a real system of movement estimation and terrain path emulation; the validation of the developed method has been carried out using reliable calculations, mathematical proofs and numerical simulations.

In summary, we have proposed a complex multimedia systems, designed for computer-human interaction, which includes several aspects of innovative and intelligent technology, for example:

- smart idea to control robots in a physical, virtual, and augmented space,
- complex virtual computer system for emulation of natural environments (variable in height) for the purposes of training (exercise and learning under supervision),
- haptic method of passing information about the direction and speed of movement of a walker (in the cyber-sphere),
- smart roll component (DME), allowing for local measurement of the speed and direction of motion of the sphere, and also for local forcing of the sphere's movement (in a different operating mode),
- intelligent processing of signals from the DME elements to estimate the direction and speed of the sphere,
- adaptation (self-tuning) based on a scheduling variable, which is the estimated direction of motion of the sphere,
- adaptive system used for control of downforce applied to the rolls in order to:
  - reduce consumption of roll surfaces,
  - control of the resistance of the movement of the sphere (in an active mode for the user), and
  - induce an adequate resistance for the sphere's movement (in a passive, simulation mode).

APPENDIX A
ANGULAR VELOCITY OF THE ROLL

Derivation of the relationship between the angular velocities of the roll and sphere begins with an energy balance equation

$$\int_{\beta-\alpha}^{\beta+\alpha} \omega_r r(\gamma) d\gamma = \int_{\beta-\alpha}^{\beta+\alpha} \omega_s R(\gamma) d\gamma \tag{30}$$

Rearranging with due regard for ω_r yields:

$$\omega_r = \frac{\omega_s \int_{\beta-\alpha}^{\beta+\alpha} R(\gamma) d\gamma}{\int_{\beta-\alpha}^{\beta+\alpha} r(\gamma) d\gamma} \tag{31}$$

Next, applying in the above the radius of the sphere $R(\gamma)$=$R_0 sin(\gamma)$, where R_0 is the maximal radius of the sphere, and the radius of the roll $r(\gamma)$=$r_0 + R_0(cos(\alpha) - cos(\beta - \gamma))$ (see Appendix B), where r_0 is the radius of the undeformed roll, one obtains:

$$\omega_r = \frac{\omega_s R_0 \int_{\beta-\alpha}^{\beta+\alpha} sin(\gamma) d\gamma}{\int_{\beta-\alpha}^{\beta+\alpha} \left(r_0 + R_0(cos(\alpha) - cos(\beta - \gamma))\right) d\gamma} \tag{32}$$

and after integration:

$$\omega_r = \frac{-\omega_s R_0 cos(\gamma)\Big|_{\gamma=\beta-\alpha}^{\gamma=\beta+\alpha}}{\left(r_0 + R_0 cos(\alpha)\right)\gamma\Big|_{\gamma=\beta-\alpha}^{\gamma=\beta+\alpha} - R_0 sin(\gamma - \beta)\Big|_{\gamma=\beta-\alpha}^{\gamma=\beta+\alpha}} \tag{33}$$

Implementing the integration limits results in:

$$\omega_r = \frac{-\omega_s \left(cos(\beta + \alpha) - cos(\beta - \alpha)\right)}{\left(\frac{r_0}{R_0} + cos(\alpha)\right) 2\alpha - sin(\alpha) + sin(-\alpha)} \tag{34}$$

Since $-sin(-\alpha)$=$sin(\alpha)$, the estimate (34) reduces to its final form:

$$\omega_r = \frac{-\omega_s \left(cos(\beta + \alpha) - cos(\beta - \alpha)\right)}{\left(\frac{r_0}{R_0} + cos(\alpha)\right) 2\alpha - 2sin(\alpha)} \tag{35}$$

APPENDIX B
RADIUS OF THE ROLL

Since the undeformed roll is assumed to have radius r_0, a formula describing the change of the radius along the contact area, when downforce is applied, is needed. Let us first assume that the roll is pushed against the sphere with such downforce that only the leftmost and the rightmost end of the roll's width remain undeformed. Such a situation is presented in Fig. 27.

For a non-zero width, the roll spans angle 2α. Assuming that the parameter γ equals zero for the middle of the roll, the sought radius has to be r_0 for γ equal to $\pm\alpha$, and r_1 for $\gamma = 0$. From Fig. 27 one can see that

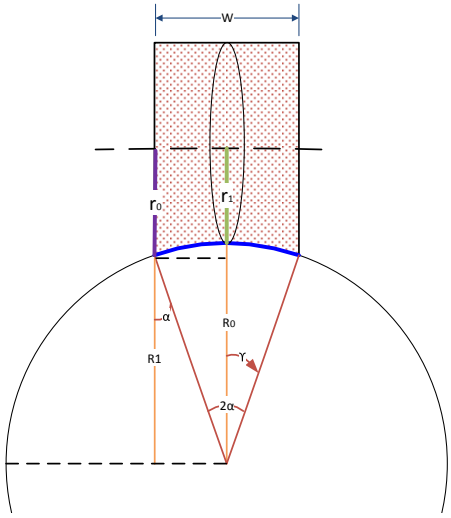

Fig. 27: Deformed roll with maximal downforce applied (R_0 is the maximum radius of the sphere, r_0 is that for the roll, 2α is the angle spanned by the roll due to its width W).

$$r_0 + R_1 = r_1 + R_0 \tag{36}$$

Since $R_1 = R_0 cos(\alpha)$, we can rewrite (36) as

$$r_0 + R_0 cos(\alpha) = r_1 + R_0 \tag{37}$$

thus

$$r_1 = r_0 + R_0(cos(\alpha) - 1) \tag{38}$$

Equation (38) holds for $\gamma = 0$. For $\gamma = \pm\alpha$, the function $r(\gamma)$ should result in r_0. To meet these requirements, we may use the following function

$$r(\gamma) = r_0 + R_0(cos(\alpha) - cos(\gamma)) \tag{39}$$

which holds for $\gamma \in < -\alpha, \alpha >$. For other values of γ within its interval, (39) acts as subtracting $R_0 cos(\gamma)$ (which yields the sum of R_1 and displacement of the roll for angle γ) from the sum of r_0 and R_1 (which is the distance of the roll's and sphere's axes, normal to them). From this, the radius of the sphere's cross-section for a given angle γ (where R_0 is the radius of the sphere's main cross-section) is obtained. Since (31) needs integration within the range $\gamma \in < \beta - \alpha, \beta + \alpha >$, other equations have to be β-invariant with respect to (39) (giving the same results). Thus the function (39 has to be rewritten for the new ranges:

$$r(\gamma) = r_0 + R_0(cos(\alpha) - cos(\beta - \gamma)) \tag{40}$$

for $\gamma \in < \beta - \alpha, \beta + \alpha >$, which yields the same results as (39) for $\gamma \in < -\alpha, \alpha >$, and can be used in further considerations.

REFERENCES

[1] A. Mazikowski and J, Lebiedź, "Image projection in Immersive 3D Visualization Laboratory", presented at *18th International Conference in Knowledge Based and Intelligent Information and Engineering Systems KES*, Gdynia, 2014, in *Procedia Computer Science 35*, 2014, pp. 842-850. [Online]. Available: http://www.sciencedirect.com/science/article/pii/S18770509140 12162.

[2] J. Lebiedź and A. Mazikowski, "Innovative Solutions for Immersive 3D Visualization Laboratory", presented at *22nd International Conference on Computer Graphics, Visualization and Computer Vision WSCG*, 2014, in *Communication Papers Proceedings*, (ed. Vaclav Skala), Plzeň, 2014, p. 315-319. [Online]. Available: http://wscg.zcu.cz/WSCG2014/!!_2014-WSCG-Communication.pdf#page=327.

[3] J. Lebiedź and A. Mazikowski, "Launch of the Immersive 3D Visualization Laboratory", in *Szybkobieżne Pojazdy Gąsienicowe*, vol. 34, no. 1, 2014. [Online]. Available: http://www.obrum.gliwice.pl/upload/downloads/spg/114/04_en _Lebiedz_Mazikowski.pdf.

[4] J. Lebiedź, J. Lubinski, A. Mazikowski, "Immersive 3d visualization laboratory concept", in: 2nd International Conference on Information Technology (ICIT), 2010, pp. 71–74.

[5] "The world in a box [the big picture]", IEEE Spectrum 52, pp. 20–21, 2015.

[6] K.E. MacLean, "Haptic Interaction Design for Everyday Interfaces", Reviews of Human Factors and Ergonomics, vol. 4(1), pp. 149-193, 2008.

[7] G. R. Luecke, "Haptic Interactions Using Virtual Manipulator Coupling With Applications to Underactuated Systems" in *IEEE Transactions on Robotics*, vol. 27, no. 4, pp. 730-740, Aug. 2011. doi: 10.1109/TRO.2011.2141210

[8] J. P. Kim, S. Y. Baek, J. Ryu, "A Force Bounding Approach for Multi-Degree-of-Freedom Haptic Interaction" in *IEEE/ASME Transactions on Mechatronics*, vol. 20, no. 3, pp. 1193-1203, June 2015. doi: 10.1109/TMECH.2014.2333537

[9] R. J. Adams, B. Hannaford, "Stable haptic interaction with virtual environments" in *IEEE Transactions on Robotics and Automation*, vol. 15, no. 3, pp. 465-474, Jun 1999. doi: 10.1109/70.768179

[10] S. A. Bowyer, F. Rodriguez y Baena, "Dissipative Control for Physical Human–Robot Interaction" in *IEEE Transactions on Robotics*, vol. 31, no. 6, pp. 1281-1293, Dec. 2015. doi: 10.1109/TRO.2015.2477956

[11] R. Cortesao, J. Park, O. Khatib, "Real-time adaptive control for haptic telemanipulation with Kalman active observers" in *IEEE Transactions on Robotics*, vol. 22, no. 5, pp. 987-999, Oct. 2006. doi: 10.1109/TRO.2006.878787

[12] M. Yaqoob, S. R. S. Qaisrani, M. W. Tariq, Y. Ayaz,S. Iqbal, S. Nisar, "Design and Control of a Haptic Enabled Robotic Manipulator" in *International Journal of Advanced Robotic Systems*, vol. 12, no. 7, July 2015.

[13] P. Hehenberger, B. Vogel-Heuser, D. Bradley, B. Eynard, T. Tomiyama, S. Achiche, "Design, modelling, simulation and integration of cyber physical systems: Methods and applications", Computers in Industry"= 82 (2016) 273–289.

[14] E. Medina, R. Fruland, S. Weghorst, "Virtusphere: Walking in a human size vr "hamster ball"", Proceedings of the Human Factors and Ergonomics Society Annual Meeting 52 (2008) 2102–2106.

[15] H. Iwata, H. Yano, H. Fukushima, H. Noma, "Circulafloor", in: ACM SIG- GRAPH 2004 Emerging Technologies, SIGGRAPH '04, ACM, New York, NY, USA, 2004, doi:10.1145/1186155.1186159.

[16] H. Iwata, H. Yano, H. Fukushima, H. Noma, "Circulafloor [locomotion interface]", IEEE Computer Graphics and Applications 25 (2005) 64–67.

[17] "Cyberith virtual interface", 2015. [Online]. Availavle: http://cyberith.com/.

[18] M. Nabiyouni, S. Scerbo, V. DeVito, S. Smolen, P. Starrin, D. A. Bowman, "Design and evaluation of a visual acclimation aid for a semi-natural locomotion device", in: 3D User Interfaces (3DUI), 2015 IEEE Symposium on, 2015, pp. 11–14. doi:10.1109/3DUI.2015.7131718.

[19] W. E. Marsh, T. Kluss, "Capturing user intent in a virtusphere", in:Proceedings of the 11th Biannual Conference on Italian SIGCHI Chapter, CHItaly 2015, ACM, New York, NY, USA, 2015, pp. 170–173. doi:10.1145/2808435.2808459.

[20] W. Tarnowski, "Lecture Notes from Basics of Machine Construction, Chapter 6: Friction gears", Koszalin University of Technology. [Online]. Available: http://wtie.tu.koszalin.pl/system/attachments/attaches/000/000/042/original/przekladnie-cierne.pdf.

[21] J. Gao, W. D. Luedtke, D. Gourdon, M. Ruths, J. N. Israelachvili and U. Landman, "Frictional forces and Amontons' law: from the molecular

to the macroscopic scale", in *The Journal of Physical Chemistry B*, vol. 108, no. 11, pp. 3410-3425, 2014.
[22] B. Bhushan, "Modern Tribology Handbook, Two Volume Set", ISBN 9780849384035, CRC Press, 2000.
[23] Y.H. Lee, H.K. Kim, H.D. Kim, C.Y. Park, I.S. Kim, "A Comparative Study on the Fretting Wear of Steam Generator Tubes in Korean Power Plants", Wear, vol. 255, pp. 1198-1208, 2003.
[24] A. Ramalho, J.C. Miranda, "The Relationship between Wear and Dissipated Energy in Sliding Systems", Wear, vol. 260, pp. 361–367, 2006.
[25] E. Sauger, S. Fouvry, L. Ponsonnet, Ph. Kapsa, J.M. Martin, L. Vincent, "Tribologically Transformed Structure in Fretting", Wear, vol. 245, pp. 39-52, 2000.
[26] X. Song, H. Liu, K. Althoefer, T. Nanayakkara, L. D. Seneviratne, "Efficient Break-Away Friction Ratio and Slip Prediction Based on Haptic Surface Exploration" in *IEEE Transactions on Robotics*, vol. 30, no. 1, pp. 203-219, Feb. 2014. doi: 10.1109/TRO.2013.2279630
[27] J. Williams, "Engineering Tribology", Cambridge University Press, 1994.
[28] P. Tomaraee, A. Mardani, A. Mohebbi and H. Taghavifar, "Relationships among the contact patch length and width, the tire deflection and the rolling resistance of a free-running wheel in a soil bin facility", in *Spanish Journal of Agricultural Research*, vol. 13, issue 2, 2015. [Online]. Available: http://dx.doi.org/10.5424/sjar/2015132-5245.
[29] Http, "The contact patch". [Online]. Available: http://the-contact-patch.com/.

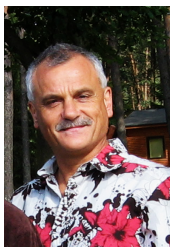

Zdzisław Kowalczuk – Prof. DSc PhD MScEE (2003, 1993, 1986, 1978). Since 1978 he has been with the Faculty of Electronics, Telecommunications and Informatics at the Gdańsk University of Technology, where he is a Full Professor in automatic control and robotics, and the Chair of the Department of Robotics and Decision Systems. He held visiting appointments at University of Oulu (1985), Australian National University (1987), Technische Hochschule Darmstadt (1989), and at George Mason University (1990-1991). Main interests include robotics, adaptive and predictive control, system modeling and identification, failure detection, signal processing, artificial intelligence, control engineering and computer science. He has authored and co-authored about books (incl. WNT 2002, Springer 2004, PWNT 2007-2016, Springer 1014) and 50 book chapters, about 100 journal papers (40 on JCR) and over 200 conference publications. He is the President of the Polish Consultants Society and of POLSPAR – the Polish Society for Measurements, Automatic Control and Robotics, the NMO of IFAC. Since 2003 professor Kowalczuk is the founder and chief editor of the publishing house PWNT – the Pomeranian Science and Technology Publishers. He is also a recipient of 1990 and 2003 Research Excellence Awards of Polish National Education Ministry, and the 1999 Polish National Science Foundation Award in automatic control, as well as the 2014 Medal of the Association of Polish Electrical Engineers SEP named after Professor Paweł Jan Nowacki.

Marek Tatara born in 1991 in Olsztyn, Poland. Lecturer at Gdańsk University of Technology, Faculty of Electronics, Telecommunications and Informatics. Currently pursuing his PhD degree in control engineering and robotics. His scientific interests concern mathematical modeling of physical processes, diagnostics, signal processing applied to industrial processes and evolutionary music composition.